Point-to-point responses

*We appreciate the reviewers for their valuable and constructive comments, which are very helpful for the improvement of the manuscript. We have revised the manuscript carefully according to the reviewers' comments. We have addressed the reviewers' comments on a point-to-point basis as below for consideration, where the reviewers' comments are cited in* ***black****, and the responses are in* ***blue****.*

## *Referee #1*

Xing et al. learned the vertical variations and sources of $O_3$ and HONO and their precursors on the Tibetan Plateau. The authors found that the contributions of HONO and $O_3$ to the production rates of OH on the TP are even greater than at lower-altitudes areas. This study will enrich the new understanding of vertical distribution of atmospheric components and explained the strong AOC on the TP. From the point of view of the data and scientific value, I recommend this manuscript being published in ACP after following revisions.

1. Authors should reorganize the abstract. The significance of the research and the most significant scientific findings should be fully presented.

Re: Thanks for your great comments. We have reorganized the abstract as following:

"The Tibetan Plateau (TP) plays a key role in regional environment and global climate change, however, the lack of vertical observation of atmospheric species, such as HONO and $O_3$, hinders a deeper understanding of the atmospheric chemistry and atmospheric oxidation capacity (AOC) on the TP. In this study, we conducted multi-axis differential optical absorption spectroscopy (MAX-DOAS) measurements at Nam Co, the central TP, to observe the vertical profiles of aerosol, water vapor ($H_2O$), $NO_2$, HONO and $O_3$ from May to July 2019. In addition to $NO_2$ mainly exhibiting a Gaussian shape with the maximum value appearing at 300-400 m, other four species all showed an exponential shape and decreased with the increase of height. The maximum values of monthly averaged aerosol (0.17 $km^{-1}$) and $O_3$ (66.71 ppb) occurred on May, $H_2O$ ($3.68\times10^{17}$ molec $cm^{-3}$) and HONO (0.13 ppb) appeared on July, while $NO_2$ (0.39 ppb) occurred on June at 200-400 m layer. $H_2O$, HONO and $O_3$ all exhibited a multi-peak pattern, and aerosol appeared a bi-peak pattern for their averaged diurnal variations. The averaged vertical profiles of OH production rates from $O_3$ and HONO all exhibited an exponential shape decreasing with the increase of height with maximum values of 2.61 ppb/h and 0.49 ppb/h at the bottom layer, respectively. The total OH production rate contributed by HONO and $O_3$ on the TP was obviously larger than that in low-altitude areas. In addition, source analysis for HONO and $O_3$ at different height layers were conducted. The heterogeneous reaction of $NO_2$ on wet surfaces was a significant source of HONO. The maximum values of HONO/$NO_2$ appeared around $H_2O$ being $1.0\times10^{17}$ molec $cm^{-3}$ and aerosol being lager 0.15 $km^{-1}$ under 1.0 km, and the maximum values usually accompanied with $H_2O$ being $1.0\text{-}2.0\times10^{17}$ molec $cm^{-3}$ and aerosol being lager 0.02 $km^{-1}$ at 1.0-2.0 km. $O_3$ was potentially sourced from south Asian

subcontinent and Himalayas through long-range transport. Our results enrich the new understanding of vertical distribution of atmospheric components and explained the strong AOC on the TP."

2.The description of the retrieval algorithm and the corresponding uncertainty analysis of vertical profiles is missing. The authors could even put them in the supplementary materials.

Re: Thanks for your great comments.

- *Vertical profile retrieval algorithm*

The atmospheric vertical profile (aerosol, $H_2O$, $NO_2$, HONO, and $O_3$) retrieval algorithm from MAX-DOAS measurements was developed based on the optimal estimation method and used radiative transfer model as the forward model (Lin et al., 2020; Liu et al., 2022; Ji et al., 2023; Xing et al., 2023). The maximum a posteriori state vector *x* is determined by minimizing the following cost function $\chi^2$.

$$\chi^2 = \left(y - F\left(x,b\right)\right)^T S_\varepsilon^{-1}\left(y - F\left(x,b\right)\right) + \left(x - x_a\right)^T S_a^{-1}\left(x - x_a\right)$$

Here, $F\left(x,b\right)$ is the forward model, which describes the measured DSCDs *y* as a function of the retrieval state vector *x* (i.e., aerosol and trace gas vertical profiles) and the meteorological parameters *b* (e.g., atmospheric pressure and temperature profiles); $x_a$ denotes the a priori vector that serves as an additional constraint; $S_\varepsilon$ and $S_a$ are the covariance matrices of *y* and $x_a$, respectively. The retrieval of vertical profiles of aerosols and trace gases were classified into two steps. Firstly, we retrieved vertical aerosol profiles based on a series of retrieved $O_4$ DSCDs at different elevation angles. Secondly, the retrieved aerosol profiles were utilized as the input parameters to the radiative transfer model to retrieve $H_2O$, $NO_2$ and HONO profiles. Considering the strong $O_3$ absorption in the stratosphere, the retrieval of the tropospheric $O_3$ profile must remove the influence of stratospheric $O_3$. In this study, daily stratospheric $O_3$ profiles from TROPOMI measurements were included in the radiative transfer model simulation for tropospheric $O_3$ profile retrieval to account for the influence of stratospheric $O_3$ absorption on the retrieval.

- *Error analysis*

The error sources can be divided into four different types: smoothing error, noise error, forward model error, and model parameter error (Rodgers, 2004). However, in terms of this classification, some errors are difficult to be calculated or estimated. For example, the forward model error, which is caused by an imperfect representation of the physics of the system, is hard to be quantified due to the difficulty of acquiring an improved forward model. Given calculation convenience and contributing ratios of different errors in total error budget, we mainly took into account following error sources, which were smoothing and noise errors, algorithm error, cross section error, and uncertainty related to the aerosol retrieval (only for trace gas). In this study, we estimated the

contribution of different error sources to the AOD and VCDs of trace gases, and near-surface (0–200 m) trace gases' concentrations and aerosol extinction coefficients (AECs), respectively. The detailed demonstrations and estimation methods are displayed below, and the corresponding varies errors are summarized in Table R1.

a. Smoothing errors arise from the limited vertical resolution of profile retrieval. Noise errors denote the noise in the spectra (i.e., the error of DOAS fits). Considering the error of the retrieved state vector equaling the sum of these two independent errors, we calculated the sum of smoothing and noise errors on near-surface concentrations and column densities, which were 13 and 5 % for aerosols, 13 and 36 % for $H_2O$, 12 and 14 % for $NO_2$, 18 and 21 % for HONO, and 12 and 32 % for $O_3$, respectively.
b. Algorithm error is denoted by the differences between the measured and simulated DSCDs. This error contains forward model error from an imperfect approximation of forward function, parameter error of forward model, and other errors, such as detector noise (Rodgers, 2004). Algorithm error is a function of the viewing angle, and it is difficult to assign this error to each altitude. Thus, this error on the near-surface values and column densities is estimated through calculating the average relative differences between the measured and simulated DSCDs at the minimum and maximum elevation angle (except 90°), respectively (Wagner et al., 2004). In this study, we estimated these errors on the near-surface values and the column densities at 4 and 8 % for aerosols, 3 and 11 % for $NO_2$, and 20 and 20 % for HONO referring to Wang et al. (2017, 2020), 1 and 8 % for $H_2O$ referring to Lin et al. (2020), and 6 and 10 % for $O_3$ referring to Ji et al. (2023), respectively.
c. Cross section error arises from the uncertainty in the cross section. According to Thalman and Volkamer, (2013), Lin et al. (2020), Vandaele et al. (1998), Stutz et al. (2000), and Serdyuchenko et al. (2014), we adopted 4, 3, 3, 5, and 2 % for $O_4$ (aerosols), $H_2O$, $NO_2$, HONO and $O_3$, respectively.
d. The profile retrieval error for trace gases is sourced from the uncertainty of aerosol extinction profile retrieval and propagated to trace gas profile. This error could be roughly estimated based on a linear propagation of the total error budgets of the aerosol retrievals. The errors of the learned four trace gases were roughly estimated at 14 % for VCDs and 10 % for near-surface concentrations, respectively.

The total uncertainty was the sum of all above errors in the Gaussian error propagation, and the error results were listed in Table R1. We found that the smoothing and noise errors played a dominant role in the total uncertainties of aerosol and trace gases. Moreover, improving the accuracy and temperature gradient of the absorption cross section is another important means to reduce the uncertainty of the vertical profiles in the future, especially for $O_3$.

**Table R1.** Error budget estimation (in %) of the retrieved near-surface (0–200 m) concentrations of trace gases and AECs, and AOD and VCDs.

| | | Error sources | | | | Total |
|---|---|---|---|---|---|---|
| | | Smoothing and noise errors | Algorithm error | Cross section error | Related to the aerosol retrieval (only for trace gases) | |
| Near-surface | aerosol | 13 | 4 | 4 | - | 14 |
| | $H_2O$ | 13 | 1 | 3 | 14 | 19 |

| | | | | | | |
|---|---|---|---|---|---|---|
| | $NO_2$ | 12 | 3 | 3 | 14 | 18 |
| | HONO | 18 | 20 | 5 | 14 | 29 |
| | $O_3$ | 12 | 6 | 2 | 14 | 19 |
| VCD or AOD | AOD | 5 | 8 | 4 | - | 10 |
| | $H_2O$ | 36 | 8 | 3 | 10 | 38 |
| | $NO_2$ | 14 | 11 | 3 | 10 | 20 |
| | HONO | 21 | 20 | 5 | 10 | 31 |
| | $O_3$ | 32 | 10 | 2 | 10 | 35 |

3.Section 2.1 emphasized HCHO, which seems to be irrelevant to this study. I suggest the authors to modificate Figure S1 to narrow the area and focus on the area around Nam Co.

Re: Thanks for your great comments. We have modified Figure S1 as following. The HCHO was removed and the study area was narrowed down.

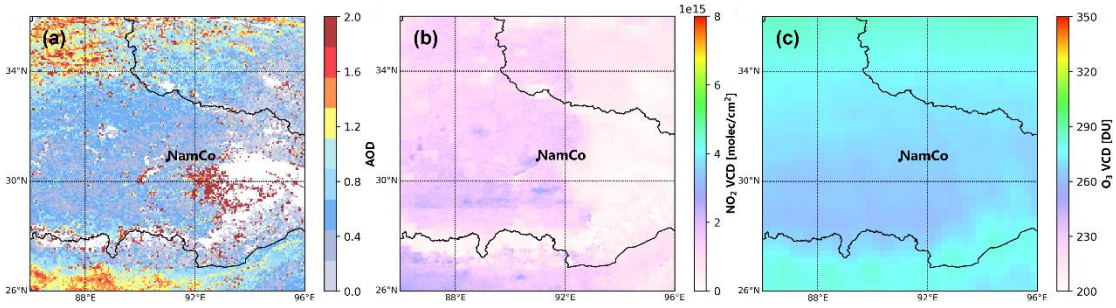


Figure R2 (S1). Averaged spatial distributions of (a) AOD monitored by Himawari-8, (b) $NO_2$ VCDs monitored by TROPOMI, (and c) $O_3$ total VCDs monitored by OMI from May to July 2019 in Nam Co.

4.The authors concluded "high concentration $NO_2$ should be attributed to the transport process from the NOx produced by ice and snow on the top of Mt. Tanggula". Can you give adequate data and literature support?

Re: Thanks for your great comments. Firstly, we added two important literatures as following to support this conclusion.

(1) Fisher F N. Extinction of UV-visible radiation in wet midlatitude (maritime) snow: Implications for increased $NO_x$ emission. Journal of Geophysical Research, 110, D21301, doi:10.1029/2005JD005963, 2005. *The main point was that snow cover in mid-latitude mountainous areas contributed significantly to $NO_x$ emissions.*

(2) Lin W, Wang F, Ye C, Zhu T. Observation of strong $NO_x$ release over Qiyi Glacier, China. The Cryosphere, doi.org/10.5194/tc-2021-32, 2021. *The main point was that high $NO_x$ production was due to photochemical reactions on the snow surface of the Tibetan Plateau.*

Secondly, we also did WPSCF analysis, and the WPSCF passing through Mt. Tanggula showed high values at 300-400 m layer, especially at 400 m (> 0.3). It indicated that the important contribution to $NO_x$ from ice and snow on the top of Mt. Tanggula under strong ultraviolet radiation.

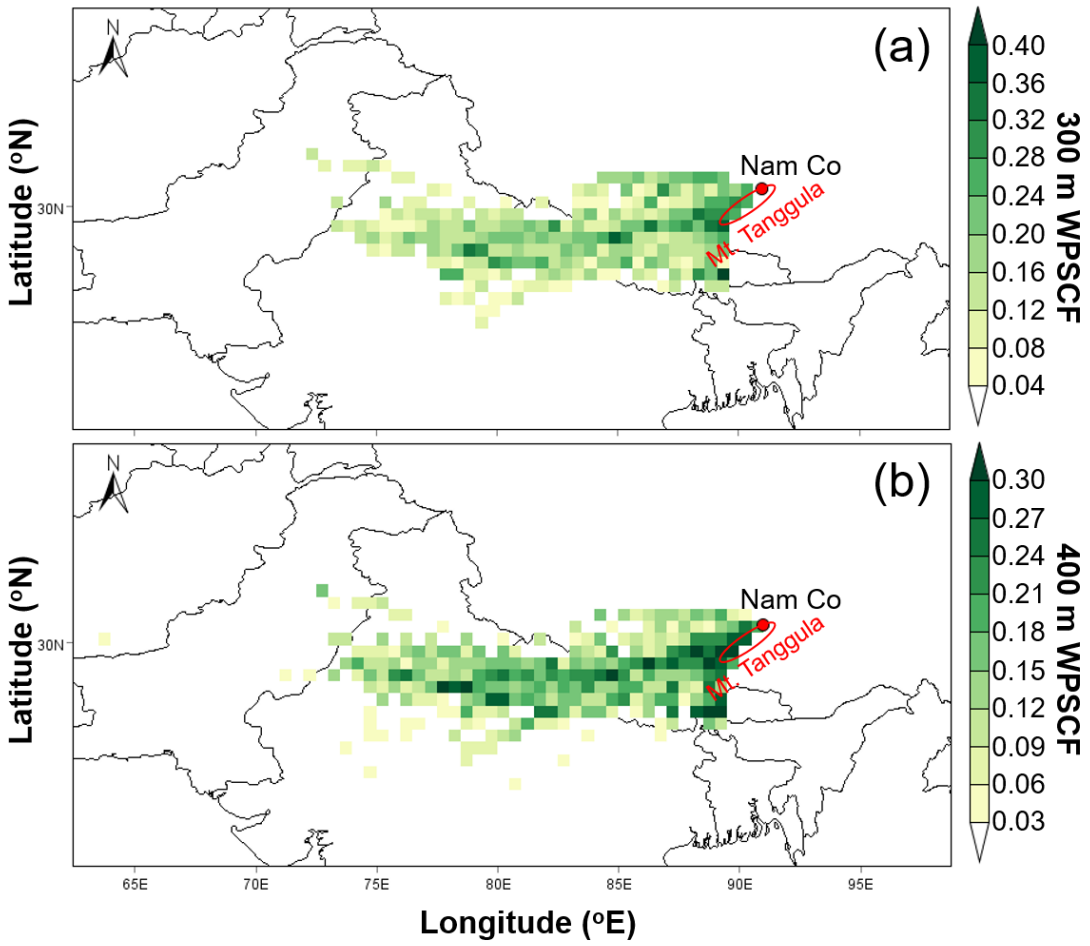


Figure R3 (S3). Spatial distributions of 24-h WPSCF values for $NO_2$ at (a) 300 m, and (b) 400 m height layers from 01 May to 09 July 2019 over CAS (NAMORS).

5. P6 L194-197, "Moreover, the large-scaled spatial distributions of AOD, $O_3$, $NO_2$ and HCHO over CAS (NAMORS) were monitored by Himawari-8 (Bessho et al., 2016), OMI (Veefkind et al., 2004) and TROPOMI (Griffin et al., 2018; Su et al., 2020), respectively."

Re: Thanks for your great comments. Referred to comment 3, we removed HCHO, and rewritten this sentence as "Moreover, the large-scaled spatial distributions of AOD, $O_3$ and $NO_2$ over CAS (NAMORS) were monitored by Himawari-8 (Bessho et al., 2016), OMI (Veefkind et al., 2004) and TROPOMI (Griffin et al., 2018; Su et al., 2020), respectively."

6. P6L202, increases > increased

Re: Thanks for your great comments. We have rewritten this sentence as "Subsequently, the AOD increases significantly, reaching maximum values during 15:00-17:00 (average of 0.107km-1), which was about 1.408 times the diurnal average value.".

7. P7L212-213, shown > was, and > but

Re: Thanks for your great comments. We have rewritten this sentence as "As shown in

Figure S2, the diurnal variation of PBL in Nam Co from May to July 2019 was lower in the early morning and late afternoon, but higher between 11:00 and 17:00 with the maximum PBL larger than 2.0 km.".

8. P12L390, first > firstly

Re: Thanks for your great comments. We have rewritten this sentence as "This phenomenon of HONO/$NO_2$ firstly increasing and then decreasing with the increasing of water vapor (or relative humidity) was usually found in low-altitude areas in previous studies (Wang et al., 2013; Liu et al., 2019; Xing et al., 2021; Xu et al., 2021).".

## *References*


Fisher F N. Extinction of UV-visible radiation in wet midlatitude (maritime) snow: Implications for increased $NO_x$ emission. Journal of Geophysical Research, 110, D21301, doi:10.1029/2005JD005963, 2005.

Lin W, Wang F, Ye C, Zhu T. Observation of strong $NO_x$ release over Qiyi Glacier, China. The Cryosphere, doi.org/10.5194/tc-2021-32, 2021.

Ji X, Liu C, Wang Y, Hu Q, Lin H, Zhao F, Xing C, Tang G, Zhang J, Wagner T. Ozone profiles without blind area retrieved from MAX-DOAS measurements and comprehensive validation with multi-platform observations. Remote Sensing of Environment, 284, 113339, doi.org/10.1016/j.res.2022.113339, 2023.

Liu C, Xing C, Hu Q, Li Q, Liu H, Hong Q, Tan W, Ji X, Lin H, Lu C, Lin J, Liu H, Wei S, Chen J, Yang K, Wang S, Liu T, Chen Y. Ground-based hyperspectral stereoscopic remote sensing network: A promising strategy to learn coordinated control of $O_3$ and $PM_{2.5}$ over China. Engineering, 19, 71-83, doi.org/10.1016/j.eng.2021.02.019, 2022.

Lin H, Liu C, Xing C, Hu Q, Hong Q, Liu H, Li Q, Tan W, Ji X, Wang Z, Liu J. Validation of water vapor vertical distributions retrieved from MAX-DOAS over Beijing, China. Remote Sensing, 12, 3193, doi.org/10.3390/rs12193193, 2020.

Xing C, Xu S, Song Y, Liu C, Liu Y, Lu K, Tan W, Zhang C, Hu Q, Wang S, Wu H, Lin H. A new insight into the vertical differences in $NO_2$ heterogeneous reaction to produce HONO over inland and marginal seas. Atmospheric Chemistry and Physics, 23, 5815-5834, doi.org/10.5194/acp-23-5815-2023, 2023.

Rodgers C D. Inverse methods for atmospheric sounding: theory and practice. Singapore-New Jersey-London-Hong: World Scientific Publishing; 2000.

Wagner T, Dix B, FriedeBurg C V, Frieß U, Sanghavi S, Sinreich R, Platt U. MAX-DOAS $O_4$ measurements: A new technique to derive information on atmospheric aerosols-Principles and information content. Journal of Geophysical Research: Atmospheres, 109, D22205, doi.org/10.1029/2004jd004904, 2004.

Serdyuchenko A, Gorshelev V, Weber M, Chehade W, Burrows J P. High spectral resolution ozone absorption cross-sections-Part 2: Temperature dependence. Atmospheric Measurement Techniques, 7, 625-636, doi:10.5194/amt-7-625-2014, 2014.

Wang Y, Lampel J, Xie P, Beirle S, Li A, Wu D, Wagner T. Ground-based MAX-DOAS observations of tropospheric aerosols, $NO_2$, $SO_2$ and HCHO in Wuxi, China, from 2011 to 2014. Atmospheric Chemistry and Physcis, 17, 2189-2215, doi.org/10.5194/acp-17-2189-2017, 2017.

Wang Y, Apituley A, Bais A, Beirle S, Benavent N, Borovski A, Bruchkouski I, Chan K L, Donner S, Drosoglou T, Finkenzeller H, Friedrich M M, Frieß U, Garcia-Nieto D, Gómez-Martín L, Hendrick F, Hilboll A, Jin J, Johnston P, Koenig T K, Kreher K, Kumar V, Kyuberis A, Lampel J, Liu C, Liu H, Ma J, Polyansky O L, Postylyakov O, Querel R, Saiz-Lopez A, Schmitt S, Tian X, Tirpitz J L, Van Roozendeal M, Volkamer R, Wang Z, Xie P, Xing C, Xu J, Yela M, Zhang C, Wagner T. Inter-comparison of MAX-DOAS measurements of tropospheric HONO slant column densities and vertical

profiles during the CINDI-2 campaign. Atmospheric Measurement Techniques, 13, 5087–5116, doi.org/10.5194/amt-13-5087-2020, 2020.
Thalman R, Volkamer R. Temperature dependent absorption cross-sections of $O_2$-$O_2$ collision pairs between 340 and 630 nm and at atmospherically relevant pressure. Physical Chemistry Chemical Physics, 15, 15371-15381, 2013.
Vandaele A C, Hermans C, Simon P C, Carleer M, Colin R, Fally S, Merienne M F, Jenouvrier A, Coquart D. Measurements of the $NO_2$ absorption cross-section from 42000 $cm^{-1}$ to 10000 $cm^{-1}$ (238–1000nm) at 220K and 294K. Journal of Quantitative Spectroscopy and Radiative Transfer, 59, 171-184, 1998.
Stutz J, Kim E S, Platt U, Bruno P, Perrino C, Febo A. UV-visible absorption cross sections of nitrous acid. Journal of Geophysical Research: Atmospheres, 105, 14585-14592, 2000.